

Optical Properties of Neural Tissue

Andrew K. Dunn

Abstract

The optical properties of neural tissues play critical roles in all types of optical imaging methods. The wavelength-dependent absorption and scattering properties of tissue influence imaging resolution, penetration depth, and often provide sources of contrast. Therefore, quantitative interpretation of imaging data requires knowledge of the optical properties of neural tissues. Light scattering in tissue arises from nanometer-scale spatial variations in refractive index and requires a thorough electromagnetic description of light propagation through this complex medium. Unfortunately, the complexity of neural tissues and the difficulty in measuring refractive index values make such a complete description unrealistic. Therefore, approximations must be made in order to characterize the light scattering properties of neural tissue. This chapter summarizes the various approaches to assess and describe the optical properties of neural tissue and discusses their role for cortical imaging.

Key words Light scattering, Light absorption, Optical properties, Monte Carlo, Finite-difference time-domain

1 Introduction

As described throughout this book, many optical techniques have been developed for imaging cortical structure and function. Each technique utilizes different sources of contrast and has different limitations in terms of spatial and temporal resolution, imaging depth, and sensitivity (see Chapter 2 in this volume). However, these techniques share a common feature: all are strongly dependent on the optical properties of the cortex. In some cases the optical properties provide the source of contrast and therefore these imaging methods capitalize on spatial and/or temporal variations in cortical optical properties to provide functional information. For other imaging methods, the optical properties impose limitations on the penetration depth or resolution of the technique. The most well-known example is the limited penetration depth of high-resolution imaging methods that arises from scattering in the cortex, which fortunately has been partially overcome by *in vivo* two-photon excited fluorescence microscopy.

Developing an improved understanding of the optical properties of neural tissue and their role in imaging of cortical function is necessary for proper interpretation of imaging data. Such an understanding is particularly important in applications such as multi-wavelength optical imaging of intrinsic signals (OIS) and diffuse optical tomography where quantitative values for hemoglobin oxygenation and volume changes are sought. These measurements are combined with a solution to an inverse problem and this solution is a strong function of the tissue optical properties [1]. In addition, development of new microscopy methods or refinement of existing techniques can be aided by a deeper understanding of optical properties.

This chapter reviews the physical origins of the optical properties of the cortex with a particular emphasis on light scattering. Some of the methods for modeling light interaction with tissue are described in the context of cortical imaging. Finally, several practical examples of the role of optical properties in cortical imaging are described.

2 Origins of Optical Properties of Neural Tissues

The optical properties of tissue are usually characterized by the degree of light scattering and absorption, both of which arise from the complex physical and biochemical structure of tissue. Structurally, cortical tissue comprises different neuronal and glial cell types, vasculature, blood cells, and a complex distribution of intracellular and extracellular proteins. The densities of neuronal cells and vasculature vary with cortical layers, and as a result, the absorption and scattering properties of cortical tissue vary spatially as well as spectrally. This structural complexity makes it very challenging to define specific scattering and absorption values for cortical tissue.

Absorption of light in neural tissues is generally the result of molecular absorption. Although a vast number of molecules and proteins contribute to the overall absorption, a few are the dominant absorbers in the visible and near-infrared spectrum. The strength of an individual chromophore is most commonly described by its molar extinction coefficient, ϵ , which has units of $\text{M}^{-1} \text{cm}^{-1}$. The dominant chromophores in neural tissue are oxy- and deoxy-hemoglobin, cytochrome-c-oxidase, water, NADH, and flavoproteins. Each of these chromophores has a unique molar extinction spectrum (Fig. 1). The total tissue absorption is described by the absorption coefficient, $\mu_a(\lambda)$ which has units of cm^{-1} . The quantity $\mu_a(\lambda)d\ell$ represents the probability that a photon of a particular wavelength will be absorbed along a distance $d\ell$. The absorption coefficient varies with wavelength and can be treated as a sum of the molar extinction coefficients of all individual chromophores weighted by their concentrations,

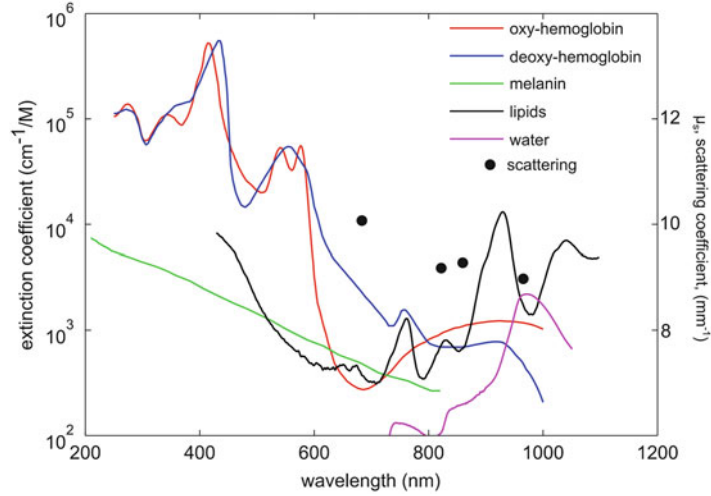


Fig. 1 Optical properties of common tissue components. The wavelength-dependent extinction coefficient ε is plotted for common tissue chromophores (*left axis*) and the scattering coefficient μ_s of neural tissue (*right axis*) is shown for four values measured from cortical tissue [2]. Note the different scales of the two axes.

$$\mu_a(\lambda) = 2.303 \sum_i \varepsilon_i(\lambda) C_i \quad (1)$$

where C_i is the concentration of a particular absorber. For wavelengths less than ~ 650 nm, oxy- and deoxy-hemoglobin are the dominant absorbers and this sum is usually truncated at two terms.

Although the absorption properties of neural tissues can be described as a linear combination of independent chromophores, the scattering properties of tissues are much more challenging to describe quantitatively. Scattering arises whenever light encounters a refractive index change. Therefore, the scattering properties of any tissue are determined by the wavelength of light and the spatial variations in refractive index. The spatial complexity of the refractive index of cortical tissue makes detailed descriptions of scattering extremely challenging. Neural tissue comprises many different cellular and noncellular structures each of which has a slightly different refractive index and size. Furthermore, most of these structures contain internal variations in refractive index that occur on the nanometer spatial scale. An exact description of the scattering properties of any tissue requires detailed knowledge of the spatial distribution of refractive index at the nanometer level, which is not feasible.

Although many studies have attempted to characterize the index of cell components, there are no definitive values for each component due to the difficulties inherent in these measurements, as well as the natural variations across cells and tissues. Table 1 summarizes some of the previously published refractive index

Table 1
Selected values of refractive index of tissue components taken from the literature.

Cell component	Refractive index	Reference
Water	1.33	[3]
Cytoplasm, rat liver cells	1.38	[4]
Mitochondria, rat liver cells	1.40	[4]
Lipid	1.48	[4]
Cytoplasm	1.35	[5]
Protein	1.50	[5]
Cytoplasm, hamster ovary cells	1.37	[6]
Mitochondria, rat liver	1.42	[7]
Melanin	1.7	[8]
Cytoplasm	1.358–1.374	[9]
Cortical cytoplasm	1.353–1.368	[10]
Dried protein	1.58	[11]

values for cellular components in general. Although many of these values are for non-neural tissues and cells, these values reveal that most organelles have refractive indices slightly above that of water.

The refractive index of cellular and noncellular components is largely determined by the local protein concentration within the component. Any component can be considered as a protein solution and its index can be written as [12]

$$n = n_0 + \alpha C \quad (2)$$

where n_0 is the refractive index of the solvent, which is approximately equal to water for cells, α is the specific refraction increment, and C is the concentration of the solute (g/100 ml). For protein, $\alpha=0.0018$, and for other solutes found in cells such as sodium, $\alpha=0.0016$ [11]. While the specific refraction increments are similar for proteins and other solutes, proteins play the largest role in determining the index of refraction because their concentrations in terms of weight per volume are considerably greater than other solutes [12].

The net scattering properties that arise from these spatial variations in refractive index are generally characterized in two ways. The first is the scattering cross section, which is a measure of the amount of light scattered by a single isolated tissue component such as a cell or organelle. The scattering cross section is related to the total amount of light scattered in all directions by a single

particle and is denoted by σ_s . Although the units of σ_s are area (m^2), the scattering cross section is not the same as the geometrical cross section of the particle and, in fact no simple relationship exists between the cross sectional area and σ_s .

While the scattering cross section is used to define the degree of light scattering from a single particle, it has limited applicability in complex tissues such as neural tissue since it is very difficult to define what comprises a single particle. The scattering cross section of objects such as microspheres and metallic nanoparticles are very useful since these particles have well-defined geometries. However, tissues contain a continuously varying refractive index on the nanometer length scale. Previous studies have characterized the scattering cross sections of biological cells and subcellular organelles [13], but it is very challenging to relate these isolated scattering cross sections to tissue level descriptions of light scattering [14].

The scattering coefficient, μ_s , is the most common measure of macroscopic, or tissue level scattering. The quantity $\mu_s dl$ represents the probability of light scattering along a distance dl , and $1/\mu_s$ represents the scattering mean free path, l_s , i.e., the average distance a photon travels between scattering events. The scattering coefficient, μ_s , is a macroscopic measure of light scattering whereas the scattering cross section, σ_s , is a microscopic or single particle measure. For discrete particles, the scattering coefficient and cross section are related by $\mu_s = \sigma_s N_v$, where N_v is the volumetric particle density (m^{-3}). For neural tissues, the scattering cross section is difficult to define due to the complex spatial composition of the tissues, and as a result, the volumetric particle density is also difficult to define. Nevertheless, the scattering coefficient, μ_s , is still a useful quantity since it is an aggregate measure of the scattering strength over a region of neural tissue.

Because in vivo measurement of absolute scattering coefficients involves complex experimental measurements that must be carefully calibrated and coupled with robust models of light propagation in tissues, significant variability exists in scattering coefficients reported in the literature. In vivo measurement of optical properties typically involves measurement of reflected intensities at multiple points along the tissue surface. The scattering and absorption properties of the tissue that give rise to these signals must then be determined by solving an appropriate inverse problem. Decoupling the contributions of skull, scalp, gray, and white matter are particularly challenging and can be aided by time- and frequency-domain measurements as well as a priori knowledge of anatomical structure [15, 16]. Therefore, the accuracy of in vivo measurement of optical properties is often determined by the accuracy of the approach used to solve the inverse problem. Ex vivo measurement of optical properties is often performed using integrating spheres that measure the diffuse reflectance and transmission of thin tissue sections as a function of wavelength. Like in vivo measurements, the integrating

sphere measurements must be combined with an appropriate inverse model to extract optical properties. These models include Monte Carlo models, analytical expressions based on the diffusion approximation, and the inverse adding doubling technique [17].

Experimental measurements of the scattering coefficient of cortex are in the range of $\mu_s = 8\text{--}12\text{ mm}^{-1}$ at wavelengths between 650 and 950 nm and show a slight decrease with increasing wavelength [2, 18]. These values correspond to a mean free path of 80–125 μm , which represents the average distance between scattering events when scattering is treated as a macroscopic process. In other words μ_s attempts to encapsulate the microscopic scattering from a volume of tissue. However, when considering very small length scales, the macroscopic interpretation of light scattering can be somewhat misleading since light cannot really travel 100 μm without any deviation. Instead, the 100 μm mean free path attempts to combine all of the very small deviations due to the microscopic variations in refractive index.

3 Optical Tissue Properties and Their Relation to Optical Imaging of Cortical Function

Both scattering and absorption can provide in vivo functional information about the cortex. One of the earliest examples of such an application was the detection of membrane potential changes by changes in light scattering in cultured neurons [19]. Dark field microscopy was used to detect the very small changes in light scattering that resulted from induced changes in transmembrane potential and a linear relationship between the scattered light intensity and membrane potential was found. The underlying mechanism was found to be a change in the radial component of the refractive index that corresponded to membrane potential. Although this study and other similar studies in slices [20, 21] established experimentally a direct change in light scattering intensity with membrane potential, the magnitude of the intensity changes is very small ($<10^{-5}/\text{mV}$). These studies have led to a renewed interest in monitoring neural activity in intact cortex through light scattering changes. One of the first reports of noninvasive detection of this signal was by Gratton et al. [22] who showed a phase shift in frequency-domain diffuse optical tomography measurements. A number of more recent studies have demonstrated that measuring such a small signal noninvasively is extremely challenging due to the very low signal to noise ratio (see [23] for a review of recent literature).

Perhaps the most widely used optical method for imaging cortical function is OIS, which indirectly measures cortical activity by detecting the hemodynamic and metabolic changes that arise from neural activity [24]. Both scattering and absorption play important

roles in these measurements. Light scattering is required to reflect light back to the camera, but it also limits the penetration depth of the measurements to the very superficial cortex. Absorption of light by oxygenated and deoxygenated hemoglobin provides the source of contrast in OIS. Therefore, the spatial and temporal dynamics of the hemodynamic response to activation can be determined qualitatively simply by examining the resulting changes in reflected light intensity. However, quantitative determination of the changes in oxy- and deoxy-hemoglobin requires measurements at multiple wavelengths and spectroscopic analysis of such measurements [25–28]. The optical properties of neural tissue play a very important role in such an analysis. In particular, both absorption and scattering effects must be accounted for. Assumptions must be made about baseline values of absorption and scattering coefficients. The absorption coefficient values are determined from the assumed baseline concentrations of oxy- and deoxy-hemoglobin. A value of the scattering coefficient and its wavelength dependence must also be assumed for calculation of the differential path length factor [27]. The controversy over the presence or absence of an initial increase in deoxy-hemoglobin during functional activation arose in part due to the role of the wavelength dependent scattering of neural tissue [25, 27].

The optical properties of neural tissues and tissue in general, particularly scattering, place constraints on the surgical preparation for most cortical imaging studies. Scattering by the skull and dura necessitates a thinned skull or full craniotomy preparation. Even when thinned skull preparations are used, mineral oil or glycerol is usually applied to the surface prior to imaging. These agents serve to improve image quality by reducing the scattering of the remaining skull. The applied oils have a relatively high refractive index that serves to reduce the spatial variations in refractive index, which in turn reduces the total scattering and improves image quality. Because scattering from the skull and cortical tissue strongly attenuates excitation light, microscopic methods such as *in vivo* two-photon imaging and confocal imaging usually require removal of the skull, although thinned-skull preparations can also be applied (see Chapter 16 in this volume). Maximum imaging depth however, is achieved by full removal of the skull or polishing the skull to transparency [29]. However, thinning the skull can reduce scattering sufficiently to allow imaging to depths of a few hundred microns while making the preparation slightly less invasive.

4 Methods for Modeling Light Propagation in Neural Tissues

Knowledge of the scattering and absorption properties of neural tissues alone is not sufficient to perform a quantitative analysis of imaging data or to predict maximum imaging depths.

For such analysis, a model of light propagation in tissue is required. Many different models have been developed and each is useful for modeling different spatial scales and measurement geometries. However, all approaches require knowledge of the scattering and absorption properties of tissue as inputs. In this section we review some of the modeling approaches that have been used and highlight how the role of optical properties of neural tissue in these models.

4.1 Monte Carlo Simulations

The Monte Carlo method for simulating light propagation in biological tissues is the most widely used modeling approach. In this approach photons are treated as particles that traverse the tissue in a stochastic process based on the radiative transport equation [30]. After tracing a large number of photons, information about reflected intensities and sampling distributions can be determined. Like all of the modeling approaches described here, results obtained from Monte Carlo simulations are only accurate when the spatial distribution and quantitative values of scattering and absorption coefficients are accurate.

Monte Carlo simulations require knowledge of the scattering coefficient, μ_s , the absorption coefficient, μ_a , and the scattering anisotropy, g , which characterizes the angular distribution of scattered light. The total attenuation coefficient, μ_t , is defined as the sum of the absorption and scattering coefficients, $\mu_t = \mu_s + \mu_a$. Anisotropy is the average cosine of the scattering angle and its values range from -1 to 1 , where a value of 1 indicates completely forward scattering, 0 indicates isotropic scattering, and -1 indicates pure backscattering. Most soft tissues have anisotropy values around 0.9 . In Monte Carlo simulations, a series of random numbers are generated to sample probability distributions that characterize photon propagation events such as scattering angle and distance between scattering events. Further details on Monte Carlo simulations of light propagation in tissues can be found in a number of reviews [31, 32].

Light propagation through complex geometries such as a human head can be modeled by assigning spatially varying scattering and absorption properties to anatomical geometries obtained with other imaging modalities such as MRI [33, 34], two-photon excited fluorescence microscopy [35], and optical coherence tomography [36, 37]. Figure 2 illustrates two examples of heterogeneous geometries used in Monte Carlo models. In one case, an anatomical MRI was segmented into different tissue types and optical properties of each tissue type were assumed [33]. In the other case, two-photon fluorescence images of cortical microvasculature were segmented to model light propagation in vascular fluorescence imaging (described in more detail below), and scattering and absorption coefficients were assigned to vascular and nonvascular tissues.

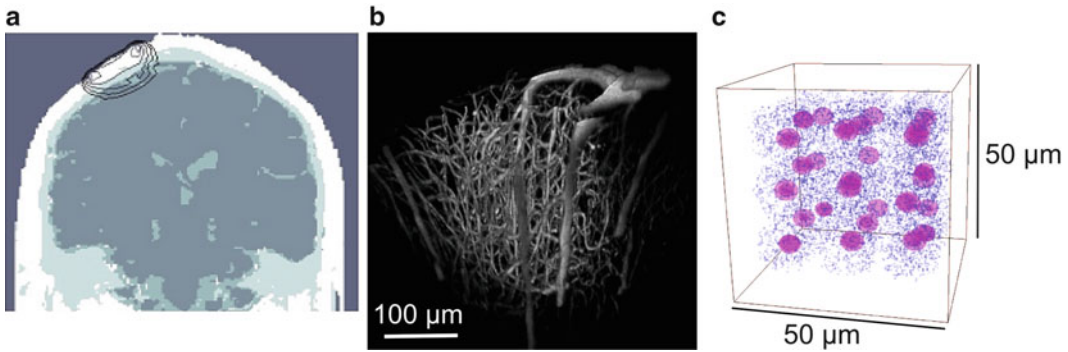


Fig. 2 Examples of geometries used in modeling light propagation through tissue. (a) Light transport through human head modeled using Monte Carlo simulations coupled with anatomical MRI data that was segmented into discrete tissue types (indicated by different *grey* levels). Scattering and absorption properties can then be assigned to each tissue type [33]. (b) Monte Carlo models can also be used to simulate light transport in invasive optical imaging geometries using segmented image stacks from two-photon microscopy as shown here. Separate optical properties can then be used for vascular and nonvascular tissues. (c) Electromagnetic modeling of light propagation enables subcellular structures to be considered assigning different refractive indices to each structure. The colors represent refractive indices ranging from 1.37–1.40 [38]. Each of the spherical structures (*magenta color*) represents cellular nuclei and the blue structures represent smaller organelles.

4.2 *Finite-Difference Time-Domain Method*

Monte Carlo simulations work well when simulating multiple scattering effects in tissues. However, when the tissue volume of interest is small, or when the effects of small-scale features such as subcellular components on light scattering are desired, Monte Carlo methods cannot usually be used. In order to properly model such small-scale features, an electromagnetic approach that takes into account the wave nature of light must be employed. Although numerous electromagnetic modeling methods have been developed, all require extensive computational resources. The most common method for modeling light scattering from complex biological tissues [13] is the finite-difference time-domain (FDTD) method [39] due to its relative simplicity and its ability to incorporate arbitrary three-dimensional spatial variations in refractive index. The FDTD method has been used extensively to solve a wide variety of electromagnetics and scattering problems [40]. This method is a full vector solution of the electric and magnetic fields in a small region surrounding an object. The electric and magnetic fields are discretized on a spatial grid and are updated in a time stepping manner. The full details of FDTD simulations can be found in a number of reviews [40].

Unlike Monte Carlo models where the macroscopic scattering and absorption coefficients are used to define the tissue, in FDTD models, the spatially varying dielectric properties (or refractive index) of tissue at the scale of a few nanometers are used to create the geometry. Absorption can be incorporated into such models by including a complex refractive index. Figure 2c illustrates an example of a three-dimensional multi-cell geometry used in an FDTD

simulation of focused beam propagation [38]. In this example, the cells are constructed from cubic voxels and the refractive index at each voxel is used to specify individual cellular components. In the example in Figure 2c nuclei of cells have a different refractive index than smaller organelles and cytoplasm. The major drawback of FDTD models, however, is the large computational demand that is required to simulate realistic tissues. The computational requirements result from the stability criteria of the finite difference approach which limits the maximum voxel size to one tenth of the wavelength of light [39]. In practice, most simulations of light scattering by biological cells use cubic voxels that are $\lambda/20$ to $\lambda/15$. Due to the need to discretize geometries with such fine resolution, two problems arise in FDTD models. First, the refractive index distribution should be known on length scales of approximately 10 nm. As discussed earlier, refractive index values are very difficult to measure and therefore, they are assumed in most models. Despite this limitation, FDTD simulations can provide detailed information about the effects of organelles on light scattering from cells [13, 14, 41] as well as the effects of cellular structures on the beam profile of focused beams [38]. The second problem is that the computational requirements for simulation of volumes of tissue that are only $\sim 50 \mu\text{m}$ on a side are extremely high. In particular, the memory requirements for such simulations require the use of distributed computing systems that can provide hundreds to thousands of gigabytes of memory [14].

5 Influence of Optical Properties on Cortical Imaging

In this section we describe several examples of how optical properties of neural tissue influence some common cortical imaging methods. These studies illustrate the strong influence of scattering and absorption on the depth sensitivity of camera-based reflectance and fluorescence methods and on the depth penetration limits of techniques such as two-photon excited fluorescence microscopy. These studies also highlight the importance of the modeling approaches described above.

5.1 Depth Sensitivity of Camera-Based Reflectance and Fluorescence Imaging of Cortex

Camera-based imaging of the cortex such as OIS, multi-wavelength OIS, laser speckle contrast imaging (see Chapters 14 and 15 in this volume), and voltage sensitive dye imaging (see Chapter 8 in this volume), provide valuable information about cortical activity on the macroscopic spatial scale (without cellular resolution). Rather than providing depth-resolved activation images, these techniques provide depth-integrated measures of cortical activation. However, the depth weighting is not a simple uniform weighting function. Instead, it is dependent on tissue optical properties, measurement

geometry, and tissue structure. In vivo experimental determination of this depth sensitivity function and the role of optical properties are exceedingly challenging. As a result, modeling studies must be performed to systematically address these issues.

One example of such a modeling study is illustrated in Box 1 [42]. In this study the role of several experimental parameters on the depth sensitivity of camera-based reflectance and fluorescence imaging was investigated using Monte Carlo simulations.

Box 1 Spatial Resolution and Depth Sensitivity of Camera-Based Intrinsic Optical Imaging.

This box describes the main findings from the Monte Carlo simulation study by [42] focused on estimation of the spatial resolution and the depth sensitivity of the camera-based 2D optical imaging methods [42].

In OIS, the measured signal (the intensity of each pixel on the CCD) is a weighted sum of the contribution from tissues at different cortical depths. The term “depth sensitivity” is used to describe this weighting function. Due to both light scattering and defocus, an array of point sources along the cortical depth results in a blurred image on the CCD. The term “spatial resolution” is used to characterize the lateral size of this image.

Both properties, i.e., spatial resolution and depth sensitivity, are determined by configurations of the imaging system (numerical aperture, NA, and focal plane depth, FPD) and optical properties of the cortical tissue (refractive index n_0 , the anisotropic factor g_0 , the scattering and absorption coefficients, μ_{s0} and μ_{a0}). Monte Carlo simulations were used to characterize the spatial resolution and depth sensitivity with optical configurations typically encountered in functional brain imaging, i.e., NA of 0.1, 0.2, and 0.4; FPD from 20 to 600 μm and tissue parameters that represent cortical gray matter in visible wavelengths up to 670 nm: n_0 , g_0 , μ_{s0} , and μ_{a0} , of 1.4, 0.9, 35, and 0.27 mm, respectively.

If the image is in focus on the cortical surface (FPD=0), then a point at the focal plane will be imaged onto a point on the detector (the CCD chip) with minimal blurring. However, if FPD>0, then an area with a certain radius around the point at the focal plane will contribute to a point on the detector; therefore, the profile on the detector will be “blurred.” The larger the focal plane depth and NA, the more blurring this will induce, thus leading to a wider profile and a lower spatial resolution, as can be seen in Fig. B1a. This analysis demonstrates that *the spatial resolution of OIS is less than or comparable to the size of cortical columns*. For example, it is less than 200 μm for NA less than 0.2 or FPD less than 300 μm , and can be as high as ~20–30 μm for FPD less than 100 μm .

For functional imaging applications with hemodynamic activity spread over hundreds of microns (with lateral size comparable to or larger than spatial resolution), *increasing NA and focal plane depth (“focusing deeper in tissue”) does not increase the contribution from deeper tissues, but rather reduces the spatial resolution* (Fig. B1b). Increasing NA and focal plane depth may improve the contribution from deeper tissues when the activity is localized

(continued)

Box 1 (continued)

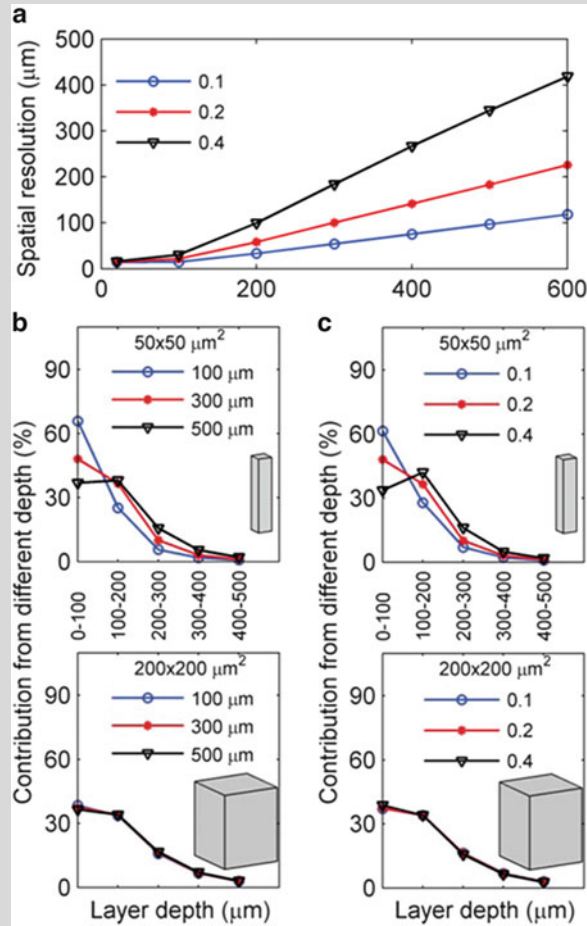


Fig. B1 Estimation of spatial resolution and depth sensitivity of OIS. **(a)** Spatial resolution versus focal plane depth for NA of 0.1 (*circle*), 0.2 (*star*), and 0.4 (*triangle*), respectively. **(b)** Depth sensitivity for functionally activated “columns” of two different cross-sectional areas: 50×50 and $200 \times 200 \mu\text{m}^2$. NA is fixed at 0.2 and the focal plane depth is varied between 100 (*blue*), 300 (*circle*), and 500 (*triangle*) μm . **(c)** The same as **(b)** but the focal plane depth is fixed at 300 μm and NA is varied among 0.1 (*circle*), 0.2 (*star*), and 0.4 (*triangle*).

within tens of microns spread in the XY plane (Fig. B1b). However, such limited spread does not naturally occur in the cerebral cortex.

More than 97 % of the OIS signal comes from the top 500 μm of the tissue, cortical layers 1 to 3. More specifically, about 38, 34, 16, 7, and 3 % of the signal are from tissues from 0–100, 100–200, 200–300, 300–400, and 400–500 μm of the cortical depths, respectively (Fig. B1b). In other words, *OIS has virtually no sensitivity to hemodynamic events deeper than 400 μm* , unless the activity propagates upstream within the arteriolar vessel wall [43].

The optical properties of the cortex also play an important role in fluorescence and phosphorescence-based measurements. A common assumption for Monte Carlo-based modeling studies is that the tissue can be approximated as a homogeneous medium. However the validity of this assumption has not been thoroughly investigated. Figure B1 shows an example of Monte Carlo simulations of camera-based fluorescence measurements in mouse cortex [35]. In these simulations the fluorescence signal was assumed to originate in the vasculature to mimic vascular fluorescence measurements. To accurately model this type of measurement, the detailed microvascular anatomy was incorporated into the simulation. The geometry was created from a stack of two photon fluorescence images of mouse cortical vasculature (blood plasma was labeled with fluorescein-dextran) that were segmented into two tissue types (vasculature and non-vasculature). Scattering and absorption properties were assigned to intra- and extravascular tissues, and a Monte Carlo model was used to propagate excitation and emission photons resulting from one photon absorption [34]. The simulated fluorescence intensity was used to calculate the spatial distribution of the origins of fluorescent signals. Vascular areas were assumed to contain a fluorophore to mimic measurements such as oxygen-dependent phosphorescence quenching [44–46] and indocyanine green fluorescence of vasculature [47]. Figure B1a and B1b shows the depth profile of the detected fluorescence signal at three different excitation wavelengths (415, 524, and 800 nm). The optical properties at each of these excitation wavelengths varied and the results indicate that for all wavelengths the majority of the detected signal originates in the first 400 μm of tissue, consistent with the results from a homogeneous geometry. However, the distribution as a function of depth is not smooth due to the heterogeneity of the cortical vasculature. Each of the peaks in the curves in Fig. 3a is the result of fluorescence contributions of single subsurface vessels. While this result may be specific to fluorescence originating only in the vasculature, it illustrates the importance of modeling with realistic geometries. Finally, Figure 3b illustrates the spatial distribution of the detected fluorescence or phosphorescence for a single pixel in a camera. Therefore, these results represent a measure of the spatial point spread function of camera-based fluorescence imaging of fluorescently labeled cortical vasculature.

5.2 Effects of Scattering on Resolution and Signal Strength in Two-Photon Imaging

As described in several chapters of this book, two-photon excited fluorescence microscopy is now a standard tool for *in vivo* investigation of many aspects of cortical function. Two-photon imaging enables a high spatial resolution and three dimensional imaging throughout much of the cortex, but the maximum penetration

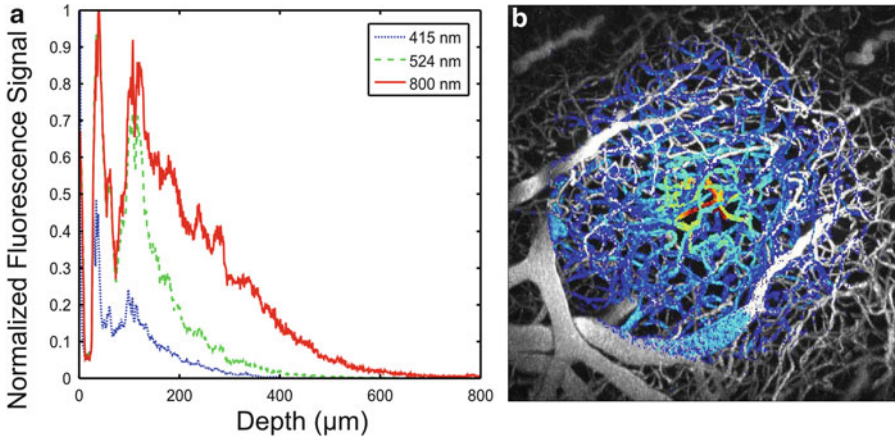


Fig. 3 Monte Carlo modeling of cortical fluorescence. **(a)** The depth dependence of fluorescence signals for camera-based imaging of fluorescently labeled cortical vasculature was modeled for visible and near-infrared fluorescent dyes with three different excitation wavelengths. **(b)** The three-dimensional geometry derived from the stack of two-photon fluorescence images shown in Fig. 2b was used. The majority of the measured fluorescence signal was found to originate in the superficial 200 μm of cortical vasculature. The three-dimensional rendering demonstrates the spatial distribution of fluorescence light for the visible and near-infrared fluorescent dyes measured by 1 camera pixel.

depth is ultimately limited by light scattering. Excitation wavelengths are in the near-infrared where scattering is lower than for single photon excitation. In addition, non-descanned detection enables detection of emission photons that have been multiply scattered. These two features enable significantly deeper imaging than with single-photon excited fluorescence confocal microscopy. Nonetheless, scattering can affect two-photon fluorescence signals in two main ways. First, scattering attenuates excitation and emission light resulting in a strong decay of signal strength with depth. Second, scattering could potentially lead to a spatial spreading of the focused beam spot leading to lower two photon absorption and degradation in spatial resolution. Experimentally, the first of these two effects has been shown to be the dominant factor. However, systematic modeling of these two effects and the role of scattering properties in signal attenuation and resolution has only been reported in a few studies [38, 48, 49].

Several Monte Carlo-based studies have investigated the role of optical properties on two-photon excited fluorescence signal levels and resolution [48–51]. These models simulate the focused beam geometry and propagate photons in a ray tracing approach that accounts for multiple scattering. Results from these studies have predicted models for signal attenuation. In particular, these simulations revealed that a single scattering event by an excitation photon is sufficient for that photon to “miss” the focal volume

and therefore, not contribute to two-photon absorption even if the angular deviation of the scattering is very small [48]. Perhaps the most significant result of these Monte Carlo studies is the result demonstrating the significant advantage in detected signal levels using high NA, low magnification objectives [49]. Such an objective maintains spatial resolution, which is only dependent on NA and wavelength. However, the combination of high NA and low magnification greatly increases the collection efficiency of fluorescence emission in scattering samples by increasing the amount of multiply scattered fluorescent photons that would be lost with high magnification or lower NA objectives. For non-scattering samples, the high NA, low magnification objectives do not provide such an advantage since the collection efficiency is only dependent on NA in the absence of scattering (Fig. B1).

The effects of scattering on the beam profile in two-photon fluorescence microscopy are more challenging to systematically investigate than the effects of scattering on signal strengths due to the need to account for diffraction. Recently, the FDTD modeling approach has been used to simulate the propagation of focused beams in tissues [38]. Although computationally costly, FDTD modeling enabled full vector solutions of Maxwell's equations for focused beam propagation through inhomogeneous biological tissues. A fifth order Gaussian beam profile was assumed for computational simplicity and the full electric and magnetic fields were determined in the focal region. The geometry consisted of a $50 \times 50 \times 50 \mu\text{m}^3$ volume containing 27 cells (Fig. 4). Each cell contained a nucleus as well as a heterogeneous distribution of smaller organelles ranging in size from 0.25 to 1.5 μm . Refractive index values for each cell component were assumed from literature values (see Table 1) and most organelles contained internal variations in refractive index. Although this tissue geometry is not specific to neural tissue, these results still provide insight into the effects of optical properties on focused beam propagation.

The two-photon excitation point spread function of the focused beam was determined by converting the steady state field distribution to intensity and squaring the resulting intensity. Figure 4 illustrates the spatial distribution of intensity when the focal plane is located approximately 42 μm into the sample. The beam appears distorted due to scattering but the beam profile through the focus remains mostly intact. This modeling study also illustrates that the central width of the excitation point spread function remains mostly constant as a function of focal plane depth, at least within the first 50 μm that were modeled. In addition, the intensity in the beam focus decayed exponentially with focal plane depth. Therefore, these results are similar to previous

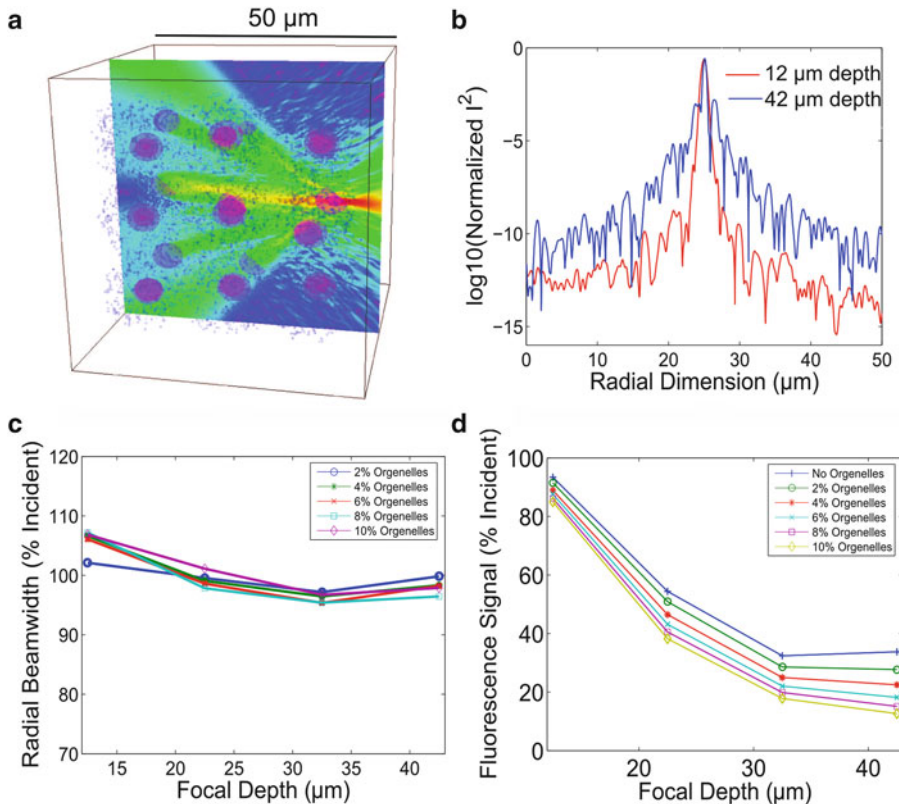


Fig. 4 Electromagnetic modeling of the effects of light scattering on beam profile of a focused laser using FDTD [38]. (a) The spatial intensity of a beam focused approximately 42 μm into a heterogeneous collection of cells. (b) The radial beam profile for two focal planes at 12 and 42 μm depth demonstrates that the width of the central lobe of the beam remains intact with increasing depth, but the intensity in the side lobes increases significantly. (c) The percent change in radial beam width shows little change with depth even as the fraction of subcellular organelles increases. (d) The integrated intensity within the focal volume, however, decreases exponentially with depth, consistent with the experimental finding that the limitation on imaging depth in two-photon fluorescence microscopy is loss of signal due to scattering rather than loss of resolution.

Monte Carlo and experimental results that scattering degrades signal strength but does not significantly affect spatial resolution. Although these FDTD studies were limited to relatively small volumes, further advances in computing power should enable full electromagnetic simulation of focused beam propagation over larger length scales.

6 Conclusions

The optical properties of neural tissue play important roles in almost all methods for imaging cortical function and structure. In some cases the optical properties provide the source of contrast, while in

other cases they limit the imaging penetration depth or resolution. In both situations it is important to understand how optical properties influence imaging data. Modeling techniques can offer important insights into the role of optical properties. However, one of the greatest limitations of modeling methods is often the uncertainty in the optical properties of neural tissue, particularly scattering. Therefore, further effort is required to obtain more conclusive values for scattering coefficients at multiple wavelengths as well as refractive index values.

References

- Villringer A, Chance B (1997) Non-invasive optical spectroscopy and imaging of human brain function. *Trends Neurosci* 20(10):435–442
- Bevilacqua F, Piquet D, Marquet P, Gross G, Tromberg B, Depeursinge C (1999) In vivo local determination of tissue optical properties: applications to human brain. *Appl Optics* 38(22):4939–4950
- Palmer KF, Williams D (1974) Optical properties of water in the near infrared. *J Opt Soc Am* 64(8):1107
- Beuthan J, Minet O, Helfman J, Muller G (1996) The spatial variation of the refractive index in biological cells. *Phys Med Biol* 41:369–382
- Kohl M, Cope M (1994) Influence of glucose concentration on light scattering in tissue. *Opt Lett* 17:2170–2172
- Brunsting A, Mullaney P (1974) Differential light scattering from spherical mammalian cells. *Biophys J* 14:439–453
- Liu H, Beauvoit B, Kimura M, Chance B (1996) Dependence of tissue optical properties on solute-induced changes in refractive index and osmolarity. *J Biomed Opt* 1:200–211
- Vitkin I, Woolsey J, Wilson B, Anderson R (1994) Optical and thermal characterization of natural (*Sepia officinalis*) melanin. *Photochem Photobiol* 59:455–462
- Lanni F, Waggoner A, Taylor D (1985) Internal reflection fluorescence microscopy. *J Cell Biol* 100:1091
- Bereiter-Han J, Fox C, Thorell B (1979) Quantitative reflection contrast microscopy of living cells. *J Cell Biol* 82:767–779
- Barer R (1957) Refractometry and interferometry of living cells. *J Opt Soc Am* 47:545–556
- Barer R, Joseph S (1954) Refractometry of living cells. *Q J Microsc Sci* 95:399–423
- Dunn A, Richards-Kortum R (1996) Three-dimensional computation of light scattering from cells. *IEEE J Sel Top Quantum Electron* 2:898–905
- Starosta MS, Dunn AK (2010) Far-field superposition method for three-dimensional computation of light scattering from multiple cells. *J Biomed Opt* 15(5):055006
- Arridge SR (1999) Optical tomography in medical imaging. *Inverse Problems* 15(2):R41–R93
- Barnett AH, Culver JP, Sorensen AG, Dale AM, Boas DA (2003) Robust inference of baseline optical properties from the human head with 3D segmentation from magnetic resonance imaging. *Appl Optics* 42:3095–3108
- Prahl SA, van Gemert MJC, Welch AJ (1993) Determining the optical properties of turbid media by using the adding-doubling method. *Appl Optics* 32(4):559
- Matcher SJ, Cope M, Delpy DT (1997) In vivo measurements of the wavelength dependence of tissue-scattering coefficients between 760 and 900 nm measured with time-resolved spectroscopy. *Appl Optics* 36(1):386–396
- Stepnoski R, LaPorta A, Raccaia-Behling F, Blonder G, Slusher R, Kleinfeld D (1991) Noninvasive detection of light changes in membrane potential in cultured neurons by light scattering. *Proc Natl Acad Sci USA* 88:9382–9386
- Cohen LB, Keynes RD, Hille B (1968) Light scattering and birefringence changes during nerve activity. *Nature* 218(5140):438–441
- Rector DM, Poe GR, Kristensen MP, Harper RM (1997) Light Scattering Changes Follow Evoked Potentials From Hippocampal Schaeffer Collateral Stimulation. *J Neurophysiol* 78(3):1707–1713
- Gratton G, Fabiani M, Friedman D, Franceschini MA, Fantini S, Corballis P, Gratton E (1995) Rapid changes of optical parameters in the human brain during a tapping task. *J Cogn Neurosci* 7(4):446–456

23. Franceschini MA, Boas DA (2004) Noninvasive measurement of neuronal activity with near-infrared optical imaging. *Neuroimage* 21(1):372–386
24. Grinvald A, Lieke E, Frostig R, Gilbert C, Wiesel T (1986) Functional architecture of cortex revealed by optical imaging of intrinsic signals. *Nature* 324:361–364
25. Malonek D, Grinvald A (1996) Interactions between electrical activity and cortical microcirculation revealed by imaging spectroscopy: implications for functional brain mapping. *Science* 272(5261):551–554
26. Mayhew J, Johnston D, Berwick J, Jones M, Coffey P, Zheng Y (2000) Spectroscopic analysis of neural activity in brain: increased oxygen consumption following activation of barrel cortex. *Neuroimage* 12(6):664–675
27. Kohl M, Lindauer U, Royl G, Kuhl M, Gold L, Villringer A, Dirnagl U (2000) Physical model for the spectroscopic analysis of cortical intrinsic optical signals. *Phys Med Biol* 45(12):3749–3764
28. Dunn AK, Devor A, Bolay H, Andermann ML, Moskowitz MA, Dale AM, Boas DA (2003) Simultaneous imaging of total cerebral hemoglobin concentration, oxygenation, and blood flow during functional activation. *Opt Lett* 28:28–30
29. Drew PJ, Shih AY, Driscoll JD, Knutsen PM, Blinder P, Davalos D, Akassoglou K, Tsai PS, Kleinfeld D (2010) Chronic optical access through a polished and reinforced thinned skull. *Nat Methods* 7(12):5–10
30. Prah S, Jacques S, Welch AJ (1989) A Monte Carlo model of light propagation in tissue. *Proc SPIE* 5:102–111
31. Wang L, Jacques SL, Zheng L (1995) MCML—Monte Carlo modeling of light transport in multi-layered tissues. *Comput Methods Programs Biomed* 47(2):131–146
32. Jacques S, Wang L (1995) Monte Carlo modeling of light transport in tissue. In: Welch AJ, Gemert MV (eds) *Optical-thermal response of laser irradiated tissue*. Plenum, New York
33. Boas DA, Culver JP, Stott JJ, Dunn AK (2002) Three dimensional Monte Carlo code for photon migration through complex heterogeneous media including the adult human head. *Opt Express* 10:159–170
34. Kumar AT, Skoch J, Bacskaï BJ, Boas DA, Dunn AK (2005) Fluorescence-lifetime-based tomography for turbid media. *Opt Lett* 30(24):3347–3349
35. Davis MA, Shams Kazmi SM, Ponticorvo A, Dunn AK (2011) Depth dependence of vascular fluorescence imaging. *Biomed Opt Express* 2(12):3349–3362
36. Pfefer TJ, Barton JK, Smithies D, Milner TE, van Gemert MJC, Nelson JS, Welch AJ (1999) Modeling laser treatment of port wine stains using a computer-reconstructed biopsy. *Lasers Surg Med* 24:151–166
37. Barton JK, Pfefer TJ, Welch AJ, Smithies DJ, Nelson J, Gemert MJV (1998) Optical Monte Carlo modeling of a true portwine stain anatomy. *Opt Express* 2:391–396
38. Starosta MS, Dunn AK (2009) Three-dimensional computation of focused beam propagation through multiple biological cells. *Opt Express* 17(15):12455–12469
39. Yee K (1966) Numerical solutions of initial boundary value problems involving Maxwell's equations in isotropic media. *IEEE Trans Antennas Propagat AP-14*:302–307
40. Taflove A (1995) *Computational electrodynamics: the finite-difference time-domain method*. Artech House, Norwood
41. Drezek R, Dunn A, Richards-Kortum R (1999) Light scattering from cells: finite-difference time-domain simulations and goniometric measurements. *Appl Optics* 38(16):3651–3661
42. Tian P, Devor A, Sakadžić S, Dale AM, Boas DA (2011) Monte Carlo simulation of the spatial resolution and depth sensitivity of two-dimensional optical imaging of the brain. *J Biomed Opt* 16(1):016006
43. Tian P, Teng IC, May LD, Kurz R, Lu K, Scadeng M, Hillman EM, De Crespigny AJ, D'Arceuil HE, Mandeville JB, Marota JJ, Rosen BR, Liu TT, Boas DA, Buxton RB, Dale AM, Devor A (2010) Cortical depth-specific microvascular dilation underlies laminar differences in blood oxygenation level-dependent functional MRI signal. *Proc Natl Acad Sci USA* 107:15246–15251
44. Sakadžić S, Yuan S, Dilekoz E, Ruvinskaya S, Vinogradov SA, Ayata C, Boas DA (2009) Simultaneous imaging of cerebral partial pressure of oxygen and blood flow during functional activation and cortical spreading depression. *Appl Optics* 48(10):D169–D177
45. Ponticorvo A, Dunn AK (2010) Simultaneous imaging of oxygen tension and blood flow in animals using a digital micromirror device. *Opt Express* 18(8):8160–8170
46. Shonat RD, Wachman ES, Niu W, Koretsky AP, Farkas DL (1997) Near-simultaneous hemoglobin saturation and oxygen tension maps in mouse brain using an AOTF microscope. *Biophys J* 73(3):1223–1231
47. Raabe A, Beck J, Gerlach R, Zimmermann M, Seifert V (2003) Near-infrared indocyanine green

- video angiography: a new method for intraoperative assessment of vascular flow. *Neurosurgery* 52(1):132–139; discussion 139
48. Dunn AK, Wallace VP, Coleno M, Berns MW, Tromberg BJ (2000) Influence of optical properties on two-photon fluorescence imaging in turbid samples. *Appl Optics* 39:1194–1201
 49. Oheim M, Beaurepaire E, Chaigneau E, Mertz J, Charpak S (2001) Two-photon microscopy in brain tissue: parameters influencing the imaging depth. *J Neurosci Methods* 111(1):29–37
 50. Gan X, Gu M (1999) Effective point-spread function for fast image modeling and processing in microscopic imaging through turbid media. *Opt Lett* 24:741–743
 51. Theer P, Denk W (2006) On the fundamental imaging-depth limit in two-photon microscopy. *J Opt Soc Am* 23(12):3139–3149